THE AMERICAN MINERALOGIST, VOL. 56, JANUARY–FEBRUARY, 1971

# VIBRATIONAL SPECTRA OF THE COMMON SILICATES: I. THE GARNETS

RAYMOND K. MOORE AND WILLIAM B. WHITE, *Materials Research Laboratory and Department of Geochemistry and Mineralogy,*

AND

THOMAS V. LONG, *Department of Chemistry, The Pennsylvania State University, University Park, Pennsylvania 16802.*

ABSTRACT

Infrared spectra have been measured on 22 specimens of silicate garnet and Raman spectra on 6 specimens. Seventeen IR modes were found as predicted by a factor group analysis. Not all of the predicted 25 Raman lines were found. The factor group splitting of the tetrahedral vibrations correlates with the occupancies of the octahedral and cubal sites. The site group splitting was used to measure the distortion of the garnet tetrahedral site.

## INTRODUCTION

The number of papers presenting infrared spectra of silicate minerals is immense. Many of these are listed in Lyon's (1962-a) bibliography. One of the most recent and complete such collections is Lyon's (1962-b) unpublished catalog of infrared spectra of silicate minerals prepared in connection with lunar exploration techniques. Interpretation of these spectra has been by mainly empirical arguments. Shifts in frequency and intensity with composition can be measured and form the most rigorous approach developed to date. This technique was applied systematically to the layer silicates by Stubican and Roy (1961) and to the olivine and spinel families independently by Tarte (1962). It has become known as the "method of isomorphous substitution."

The justifications for beginning a new round of refinements on the vibrational spectra of the common silicates are the following:

1. Infrared data can now be obtained in the range of 400–50 $cm^{-1}$ thus providing information on the low-frequency vibrations not usually available in the earlier studies.

2. Measurement of the Raman spectra yields a whole new set of information which, in centro-symmetric crystals, is nonoverlapping with any of the infrared frequencies.

3. Theoretical methods can be used which will predict the number and selection rules of all vibrational modes.

This paper presents vibrational spectra and interpretation for silicate minerals with the garnet structure. The high symmetry and presence of only isolated $SiO_4$ tetrahedra in garnet make the theoretical analysis of

the vibrations more useful than would be the case with most other silicates.

Compared with other silicates, the infrared spectra of silicate garnets have been little investigated. Only the recent paper by Griffith (1969) reports the Raman spectra of the silicate garnets. Infrared spectra have been reported by Launer (1952), Wickersheim, Lefever, and Hanking (1960), Wickersheim (1961) and Tarte (1965). The first two papers deal qualitatively with spectra in the range 650 to 1200 $cm^{-1}$ in which only two to five of the infrared bands are observed. Wickersheim (1961) presents the infrared spectrum of one natural silicate garnet (almandine) in the range 250 to 1200 $cm^{-1}$ and the spectra of impurity $SiO_4$ bands in YIG in the range 600 to 1000 $cm^{-1}$. Tarte's paper is the most comprehensive and presents spectra (in the range of 300 to 1000 $cm^{-1}$) of a large number of natural silicate garnets (including high-titanium garnets) as well as that of synthetic germanate garnets. Only qualitative interpretations were attempted on an incomplete set of bands.

Investigations of the infrared spectra of the yttrium and rare earth garnets have been carried out by Wickersheim (1961) and McDevitt (1969). Excellent papers on rare earth garnets utilizing factor group and site group methods for the analysis of Raman spectra have been published very recently. (Hurrell, Porto, Chang, Mitra, and Bauman, 1968, Koningstein and Toaning-Ng, 1968, and Koningstein and Mortensen, 1968).

## Experimental Methods

A suite of 19 garnets of varying composition was assembled. Elemental analyses were performed by emission spectrographic methods, and ferrous/ferric ratio determined by wet analytic methods. Cell edges and refractive indices were measured. The chemical composition was normalized into mole ratios of the three dominant end members of the pyrope (Py)-almandine (Al)-spessarite (Sp) series and the grossularite (Gr)-andradite (An)-uvarovite (Uv) series. A code name was attached to each specimen according to the dominant end member. The code names, the cell edges, and the molecular proportions are listed in Table 1. These same garnet crystals were used to investigate the optical spectra of the transition metal ions and full details of the characterization are reported there (Moore and White, in preparation).

Specimens for infrared measurements were ground to fine powders. Spectra in the range of 2000–300 $cm^{-1}$ were obtained on a Perkin Elmer Model 621 spectrophotometer using the powders vacuum-pressed into KBr discs. Spectra in the range of 600–50 $cm^{-1}$ were obtained on a Beckmann IR-11 spectrophotometer from powders slurried directly onto polyethylene slabs.

Raman spectra were measured from 2–3 mm cubes of single crystal oriented to have {100} faces. A Spex model 1400 double monochromator was used with a 30 mW Spectra-Physics Model 112 He-Ne laser as a source. The He-Ne excitation wavelength of 6328 Å occurs in a transmission window of the optical spectrum. Measurement of the Raman spectra of iron-containing garnets would have been very difficult with conventional sources because of the high absorbance in the blue. Polarization measurements were made by in-

TABLE 1. LATTICE PARAMETER AND MOLECULAR PROPORTIONS OF THE END-MEMBERS FOR EACH SPECIMEN

| Sample | Lattice parameter | Py | Al | Sp | Gr | An | Uv |
|---|---|---|---|---|---|---|---|
| Al-77 | 11.499 | 18.0 | 77.0 | — | 4.6 | 0.4 | — |
| Al-76 | 11.521 | 8.0 | 76.0 | 3.6 | 13.0 | — | — |
| Al-68 | 11.533 | 22.6 | 67.8 | 5.0 | 3.3 | 1.3 | — |
| Al-67 | 11.523 | 23.0 | 67.5 | 3.0 | 6.4 | — | — |
| Al-51 | 11.530 | 33.6 | 51.0 | 0.9 | 13.1 | 1.4 | — |
| Py-71 | 11.525 | 71.4 | 16.0 | 0.9 | 3.4 | 1.0 | 7.3 |
| Py-59 | 11.502 | 59.1 | 37.5 | 1.7 | 1.7 | — | — |
| Sp-70 | 11.607 | 6.8 | 22.4 | 70.0 | — | 0.8 | — |
| Sp-53 | 11.571 | 0.9 | 45.5 | 53.0 | 0.7 | — | — |
| Gr-92 | 11.844 | 3.1 | 0.5 | — | 92.0 | 4.6 | — |
| Gr-92B | 11.848 | 3.0 | 0.7 | — | 92.1 | 4.4 | — |
| Gr-90 | 11.843 | — | 3.2 | 0.6 | 89.9 | 6.4 | — |
| Gr-89 | 11.847 | — | 4.3 | 0.5 | 89.0 | 6.3 | — |
| Gr-87 | 11.843 | — | 6.0 | 0.6 | 87.3 | 6.4 | — |
| Gr-74 | 11.857 | 0.5 | 4.7 | 2.6 | 73.6 | 18.4 | — |
| An-94 | 12.033 | 1.2 | — | 0.5 | 4.5 | 94.0 | — |
| An-93 | 12.049 | — | 1.0 | 0.5 | 5.5 | 93.0 | — |
| AnTi-84 | 12.101 | 4.0 | — | 0.4 | 11.5 | 84.0 | — |
| Uv-44 | 11.920 | 6.6 | — | 1.4 | 29.0 | 19.0 | 44.0 |

serting a half-wave plate in the laser beam and rotating a polarizer placed between the polarization scrambler and the entrance slit.

## RESULTS

*Infrared Spectra.* The IR spectra of all pyralspites are similar, as are the spectra of all ugrandites. Typical examples, the spectrum of an almandine, Al-77, and an andradite, An-93 are shown in Figure 1. The bands are given a simple alphabetical label for identification. Band frequencies for all 19 specimens are listed in Table 2. Two weak bands appear between the D and E bands in the high-titanium and high-chromium garnets. Other than these, a maximum of 17 bands are observed in the infrared.

No previous author has examined the full infrared range for the natural silicate garnets; the most complete previous work is that of Tarte (1965) in which he reports twelve bands in the range 300 to 4000 $cm^{-1}$. The same number of bands was found in this range in the present study.

Hurrel *et al.* (1968) obtained the infrared spectrum of yttrium aluminum garnet over the entire infrared range and observed a total of fifteen

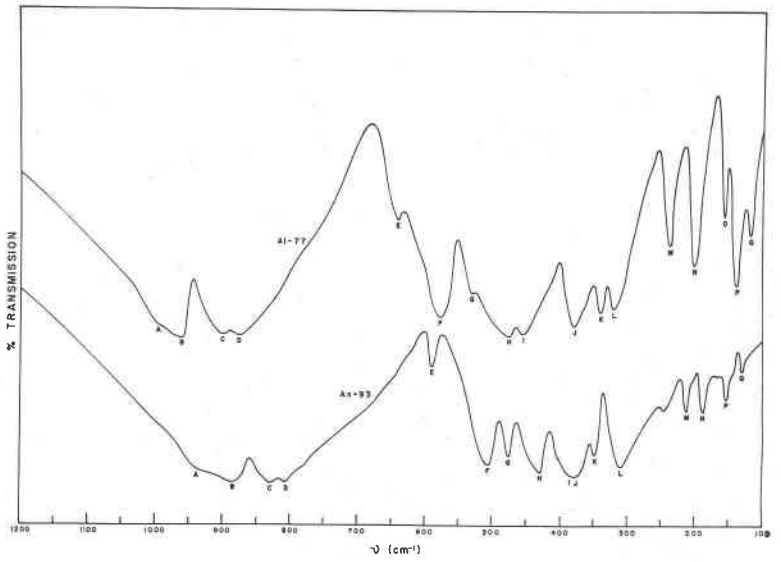


FIG. 1. Typical infrared spectra for an almandine (Al-77) and an andradite (An-93). The letter code on the bands refers to Table 2.

bands. They postulated that the two missing bands are weak and possibly degenerate with other modes. Their data for YAG are also listed in Table 2.

*Raman Spectra.* Only six samples were examined by Raman experiments. The band frequencies are presented in Table 3. The spectra of samples Al-68 and An-93 as typical examples are shown in Figure 2. A maximum of twenty bands were observed in the spectra (Gr-90).

Koningstein and Mortensen (1968) report the Raman spectra of YAG, YbAG and YGaG at room temperature and 100°K. They observed a maximum of 22 bands in the YAG sample. Koningstein and Toaning-Ng (1968) obtained the spectrum of a Thulium Gallium Garnet at 80–85°K and observed a maximum of 12 bands. Hurrel *et al.* (1968) obtained the spectrum of YAG at 90°K and observed all but three of the predicted 25 modes. In the latter two papers, polarization data for the Raman spectra were obtained and bands were assigned to particular irreducible representations.

## THEORETICAL ANALYSIS

*The Factor Group Method.* The first necessity in analyzing the garnet spectra is to determine the number of vibrational modes and the selection

TABLE 2. INFRARED BAND FREQUENCIES (IN $CM^{-1}$) FOR ALL SPECIMENS MEASURED

| Band | Al-77 | Al-76 | Al-68 | Al-67 | Al-51 | Py-71 | Py-59 | Sp-70 | Sp-53 | Gr-92 | Gr-92B | Gr-90 | Gr-89 | Gr-87 | Gr-74 | An-94 | An-93 | Uv-44 | AnTi-84 | YAG[a] |
|---|---|---|---|---|---|---|---|---|---|---|---|---|---|---|---|---|---|---|---|---|
| A | 991 | 990 | 988 | 990 | 987 | 995 | 996 | 976 | 983 | 951 | 952 | 948 | 951 | 956 | 950 | 929 | 929 | 961 | 924 | — |
| B | 960 | 962 | 960 | 960 | 961 | 965 | 964 | 949 | 951 | 905 | 907 | 911 | 912 | 915 | 910 | 888 | 888 | 899 | 866 | 812 |
| C | 897 | 897 | 899 | 896 | 896 | 897 | 897 | 895 | 888 | 852 | 855 | 858 | 858 | 860 | 854 | 831 | 831 | 839 | 826 | 738 |
| D | 870 | 873 | 863 | 870 | 869 | 870 | 870 | 861 | 863 | 834 | 835 | 840 | 841 | 841 | 835 | 812 | 811 | 826 | 810 | 690 |
| | — | — | — | — | — | — | — | — | — | 750 | 754 | — | — | — | — | — | — | 748 | 734 | — |
| | — | — | — | — | — | — | — | — | — | — | — | — | — | — | — | — | — | 675 | 670 | — |
| E | 635 | 636 | 636 | 638 | 640 | — | — | 631 | 631 | 617 | 617 | 619 | 619 | 619 | 616 | 591 | 589 | 617 | 589 | 570 |
| F | 571 | 571 | 569 | 570 | 574 | 580 | 577 | 565 | 565 | 540 | 539 | 544 | 547 | 553 | 543 | 512 | 510 | 542 | 513 | 521 |
| G | 526 | 528 | 526 | 526 | 528 | 536 | 530 | 495 | 521 | 502 | 502 | 500 | 505 | 505 | 502 | 479 | 477 | 484 | 477 | 483 |
| H | 469 | 476 | 475 | 478 | 481 | 492 | 481 | 470 | 471 | 476 | 471 | 473 | 471 | 478 | 471 | 439 | 438 | 463 | 435 | 467 |
| I | 448 | 452 | 451 | 452 | 457 | 458 | 455 | 447 | 447 | 445 | 442 | 451 | 450 | 453 | 445 | — | 400 | 432 | 398 | 430 |
| J | 376 | 377 | 378 | 378 | 381 | 386 | 379 | 379 | 377 | 385 | 387 | 393 | 392 | 390 | 387 | 390 | 383 | 375 | 385 | 392 |
| K | 338 | 339 | 340 | 340 | 342 | 345 | — | 341 | 342 | — | — | 347 | 345 | — | 343 | 352 | 348 | — | 345 | 371 |
| L | 317 | 316 | 317 | 314 | 324 | — | 327 | 308 | 314 | — | — | — | — | — | 296 | 309 | 310 | — | 308 | 330 |
| M | 237 | 238 | 236 | 234 | 240 | 248 | 243 | 242 | 240 | 238 | 240 | 240 | 240 | 241 | 236 | 211 | 211 | 229 | 215 | 290 |
| N | 192 | 200 | 199 | 197 | 203 | 209 | 196 | 203 | 210 | 200 | 202 | 203 | 202 | 203 | 200 | 186 | 187 | 198 | 187 | 219 |
| O | 156 | 159 | 157 | 157 | 160 | — | — | 165 | — | 180 | 179 | 183 | 183 | 183 | 179 | — | — | 170 | — | 165 |
| P | 137 | 138 | 137 | 137 | 140 | 149 | 141 | 140 | 138 | — | — | — | 140 | — | 153 | 133 | 132 | — | 127 | 120 |
| Q | 116 | 116 | 116 | 115 | 119 | — | 125 | 113 | 112 | — | — | — | 117 | — | 125 | 113 | — | — | — | — |

[a] Spectrum of yttrium aluminum garnet from Hurrel et al. (1968).

TABLE 3. RAMAN SHIFTS (IN $CM^{-1}$) OF GARNETS

| Band | Al-77 | Al-68 | Al-67 | Sp-70 | Gr-90 | An-93 |
|---|---|---|---|---|---|---|
| 1 | 917 | 918 | 890 | 896 | 888 | 875 |
| 2 | 839 | 841 | 843 | — | 859 | 844 |
| 3 | 796 | 798 | 806 | — | 826 | 816 |
| 4 | — | — | — | — | 759 | 751 |
| 5 | 749 | 748 | 745 | 743 | 734 | 728 |
| 6 | — | — | 695 | — | 695 | 700 |
| 7 | 665 | 659 | 644 | — | 662 | 679 |
| 8 | 625 | — | — | — | 638 | 659 |
| 9 | — | 600 | 611 | 617 | 592 | 631 |
| 10 | 566 | 571 | 562 | — | 570 | 581 |
| 11 | — | — | — | — | 557 | 562 |
| 12 | — | — | — | — | 533 | 552 |
| 13 | 505 | 509 | 517 | 503 | 516 | 501 |
| 14 | — | — | 468 | — | 483 | 476 |
| 15 | — | — | 400 | — | 426 | 461 |
| 16 | — | — | — | — | 416 | 425 |
| 17 | — | 390 | — | — | 378 | 373 |
| 18 | — | — | — | — | 348 | 358 |
| 19 | — | — | — | — | 330 | 317 |
| 20 | — | — | 307 | — | 312 | — |
| 21 | — | — | — | — | 287 | — |
| 22 | — | — | 266 | — | 257 | 241 |
| 23 | — | — | — | — | 160 | — |
| 24 | — | — | — | — | 128 | — |

rules that control them. Crystalline solids that do not contain well defined molecular units can best be analyzed by the factor group method. Factor group analysis takes into account all atoms in the solid whereas the more commonly used site group method [*cf.* Duke and Stephens (1964) for an analysis of the vibrations of the isolated $SiO_4$ groups in olivine using the site group method] accounts only for the motions of the molecular units. Although factor group analysis is commonly used in the Physics literature for analysis of the vibrational spectra of crystals, it is difficult to point to a satisfactory review article. Mitra and Gielisse (1964) and White and DeAngelis (1967) discuss the method in some detail. For a complete mathematical treatment see Maradudin and Vosko (1968).

*Application to the Garnet Structure.* Garnet is cubic, space group $Ia3d(O_h^{10})$, with $8A_3B_2(CO_4)_3$ units per unit cell. The smallest Bravais cell is primitive with 4 formula units per unit cell. In the garnet structure the A atoms are 8-fold coordinated with $D_2$ site symmetry, the B atoms

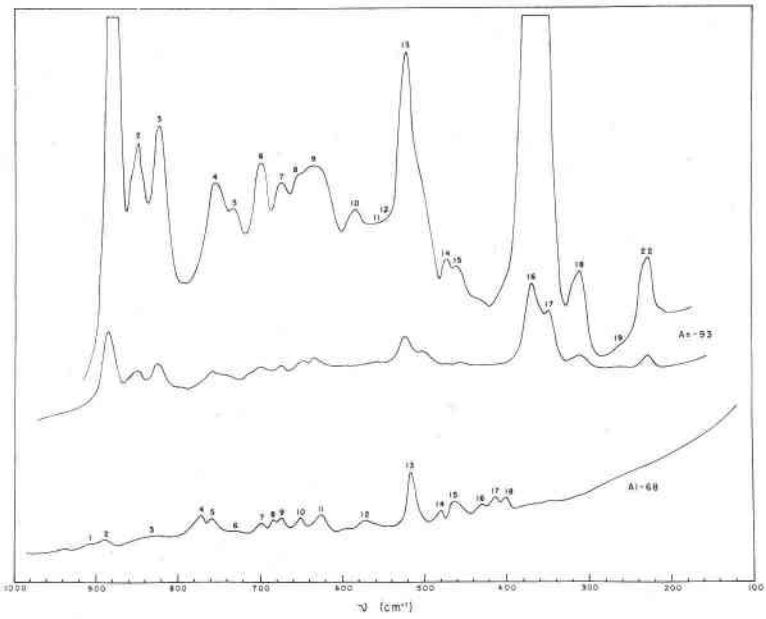


FIG. 2. Raman spectra for an almandine (Al-68) and an andradite (An-93). The two spectra of andradite represent two intensity settings of the spectrometer. The numbers on the bands refer to Table 3.

are 6-fold coordinated with $S_6$ site symmetry, and the C atoms (primarily Si) are 4-fold coordinated with $S_4$ site symmetry.

There are $3n$ degrees of freedom in a crystal, where $n$ is the number of atoms in the unit cell. The full body-centered cell contains 480 degrees of freedom or 240 degrees of freedom in the primitive cell. It is convenient to perform the analysis on the full cell with factor group $O_h$.

The invariance conditions for the atoms in the garnet structure and the reducible representations are tabulated in Table 4. From the reducible representation of the primitive cell, the vibrational degrees of freedom are classified among the irreducible representations of the factor group in Table 5. Seventeen infrared and twenty-five Raman active modes are predicted by the selection rules. Similar methods of classifying the normal modes for the garnet structure were apparently used by Hurrel *et al.* (1968), and Koningstein and Mortensen (1968).

*Site Group Analysis.* The complete factor group analysis yields the true symmetry of the various normal modes and the correct selection rules, but it is not very instructive when one wants to assign the normal modes to specific atomic motions.

TABLE 4. INVARIANCE CONDITIONS FOR GARNET SPACE GROUP $Ia3d$, $O_h^{10}$

| $O_h$ | $E$ | $8C_3$ | $6C_2$ | $6C_4$ | $3C_2$ | $i$ | $6S_4$ | $8S_6$ | $3\sigma_h$ | $6\sigma_d$ |
|---|---|---|---|---|---|---|---|---|---|---|
| $a$-site, $S_6$ | $E$ | $C_3, C_3^2$ | — | — | — | $i$ | — | $S_6^5, S_6$ | — | — |
| $\omega_p$ (16Al) | 16 | 4 | 0 | 0 | 0 | 16 | 0 | 4 | 0 | 0 |
| $d$-site, $S_4$ | $E$ | — | — | — | $C_2$ | — | $S_4, S_4^3$ | — | — | — |
| $\omega_p$ (24Si) | 24 | 0 | 0 | 0 | 8 | 0 | 8 | 0 | 0 | 0 |
| $c$-site, $D_2$ | $E$ | — | $C_{2(z)}, C_{2(y)}$ | — | $C_{2(x)}$ | — | — | — | — | — |
| $\omega_p$ (24Ca) | 24 | 0 | 8 | 0 | 8 | 0 | 0 | 0 | 0 | 0 |
| $h$-site, $C_1$ | $E$ | — | — | — | — | — | — | — | — | — |
| $\omega_p$ (96O) | 96 | 0 | 0 | 0 | 0 | 0 | 0 | 0 | 0 | 0 |
| $\omega_p$ | 160 | 4 | 8 | 0 | 16 | 16 | 8 | 4 | 0 | 0 |
| $\chi_p$ | 480 | 0 | −8 | 0 | −16 | −48 | −8 | 0 | 0 | 0 |
| $\Gamma_{RED} = \chi_{p/2}$ | 240 | 0 | −4 | 0 | −8 | −24 | −4 | 0 | 0 | 0 |

The garnet structure contains discreet $SiO_4$ tetrahedra which behave nearly independently of the other components of the structure. The binding of the $SiO_4$ tetrahedra by the 6- and 8-fold cations can be considered weak compared to the binding of the Si–O bonds themselves. This model, although only a very rough approximation in the garnet

TABLE 5. CLASSIFICATION AND SELECTION RULES FOR FUNDAMENTAL MODES OF GARNET

| $O_h$ | $N_T$ | Acous. | Translatory[a] | | | Trans.[b] | Rotatory | ($SiO_4$) Internal | Selection rules |
|---|---|---|---|---|---|---|---|---|---|
| | | | $S_4$ | $D_2$ | $S_6$ | | | | |
| $A_{1g}$ | 3 | 0 | 0 | 0 | 0 | 0 | 1 | 2 | Raman |
| $A_{2g}$ | 5 | 0 | 1 | 1 | 0 | 2 | 0 | 3 | Inactive |
| $E_g$ | 8 | 0 | 1 | 1 | 0 | 2 | 1 | 5 | Raman |
| $T_{1g}$ | 14 | 0 | 2 | 3 | 0 | 5 | 3 | 6 | Inactive |
| $T_{2g}$ | 14 | 0 | 3 | 2 | 0 | 5 | 2 | 7 | Raman |
| $A_{1u}$ | 5 | 0 | 1 | 0 | 1 | 2 | 0 | 3 | Inactive |
| $A_{2u}$ | 5 | 0 | 0 | 1 | 1 | 2 | 1 | 2 | Inactive |
| $E_u$ | 10 | 0 | 1 | 1 | 2 | 4 | 1 | 5 | Inactive |
| $T_{1u}$ | 18 | 1 | 3 | 3 | 3 | 8 | 2 | 7 | Infrared |
| $T_{2u}$ | 16 | 0 | 2 | 2 | 3 | 7 | 3 | 6 | Inactive |

[a] Translatory motions of individual cation sub-lattices.

[b] Total translatory modes = sum of $S_4 + D_2 + S_6$.

structure, can be used as a starting point to determine the behavior of independent $SiO_4$ tetrahedra.

Using this model, the number of translatory (essentially cation motions), rotatory (tetrahedral rocking motions) and internal degrees of freedom (tetrahedral independent motions) are:

| *Units* | *Internal* | *Translatory* | *Rotatory* |
|---|---|---|---|
| $12(SiO_4)$ | 108 | 36 | 36 |
| $8B$ | 0 | 24 | 0 |
| $12A$ | 0 | 36 | 0 |

The classification of each type of mode is given in Table 5.

The site symmetry of the tetrahedral site in garnet is $S_4$ whereas the normal molecular group is $T_d$. It is possible therefore to determine the site splitting or removal of degeneracy by a descent in symmetry method:

| *Mode* | $T_d$ | $S_4$ |
|---|---|---|
| $\nu_1$ | $12A_{1g}$ | $12A$ |
| $\nu_2$ | $12E_g$ | $12A+12B$ |
| $\nu_3$ | $12T_{2g}$ | $12B+12E$ |
| $\nu_4$ | $12T_{2g}$ | $12B+12E$ |

The degeneracies of the $T_d$ modes are removed to some extent by the lowering of the symmetry of the site. In addition, the selection rules are changed. Therefore in the limiting case where the tetrahedra act independently of the lattice, we would expect 5 IR active internal modes and 9 Raman active internal modes.

By the reversal of the above process the factor group representations to which these internal modes belong can be determined. An example of this method for $\nu_1$ mode is given below:

| *Mode* | $S_4$ | $T_d$ | $O_h$ |
|---|---|---|---|
| $\nu_1$ | $12A$ | $2A_{1g}$ | $A_{1g}$, $A_{2u}$ |
| | | $2E_g$ | $E_g$, $E_u$ |
| | | $2T_{1g}$ | $T_{1g}$, $T_{2u}$ |

This information for all tetrahedral modes is summarized in Table 6.

## Assignments

*Raman Spectra.* The assignments of the Raman spectra were based on polarization data obtained from a single crystal of sample Gr-90. The crystal was cut into a cube with {001} faces. The crystal was placed in the sample holder such that the incident beam direction was parallel to a crystallographic axis, and the scattered radiation parallel to an orthogonal axis. Polarizers were inserted in the incident beam and in the

TABLE 6. INTERNAL MODE DISTRIBUTION

| $O_h$ | Internal | $\nu_1$ | $\nu_2$ | $\nu_3$ | $\nu_4$[a] |
|---|---|---|---|---|---|
| $A_{1g}$ | 2 | 1 | 1 | 0 | 0 |
| $A_{2g}$ | 3 | 0 | 1 | 1 | 1 |
| $E_g$ | 5 | 1 | 2 | 1 | 1 |
| $T_{1g}$ | 6 | 1 | 1 | 2 | 2 |
| $T_{2g}$ | 7 | 0 | 1 | 3 | 3 |
| $A_{1u}$ | 3 | 0 | 1 | 1 | 1 |
| $A_{2u}$ | 2 | 1 | 1 | 0 | 0 |
| $E_u$ | 5 | 1 | 2 | 1 | 1 |
| $T_{1u}$ | 7 | 0 | 1 | 3 | 3 |
| $T_{2u}$ | 6 | 1 | 1 | 2 | 2 |

[a] $\nu_1$, $\nu_2$ etc. are Herzberg's (1945) notation for the vibrational motions of a regular tetrahedral molecule. $\nu_1$ is the symmetric stretch, $\nu_2$ the symmetric bend, $\nu_3$ the antisymmetric stretch, and $\nu_4$ the antisymmetric bend.

scattered beam. By rotating the analyzer 90° the polarizability components of the scattered radiation could be observed parallel and perpendicular to the plane of polarization of the incident beam. These two experimental conditions are summarized by the notation $x(yy)z$ and $x(yx)z$ (This notation is due to S. P. S. Porto and is widely used). The two letters inside the brackets represent the directions of polarization for the incident and scattered beams respectively, and the letters outside the brackets represent the direction of the incident and scattered beams respectively. Under the experimental conditions, the $A_{1g}$ and $E_g$ modes are observable under parallel polarizers but not under crossed polarizers, while the $T_{2g}$ modes are observable under crossed, but not parallel polarizers. A summary of the experimental conditions for the observation of these modes is presented in Table 7.

Examples of the polarized spectra are presented in Figure 3. The $A_{1g}$ and $E_g$ modes do not completely extinct when the polarizers are

TABLE 7. POLARIZABILITY COMPONENTS AND CONDITIONS FOR THE EXPERIMENTAL OBSERVATION OF THE RAMAN MODES

| Mode | Polarizability component | Experimentally observable | |
|---|---|---|---|
| | | $y(xx)z$ | $y(xy)z$ |
| $A_{1g}$ | $xx$, $yy$, $zz$ | yes | no |
| $E_g$ | $yy$, $xx+yy-2zz$ | yes | no |
| $T_{2g}$ | $xy$, $xz$, $yz$ | no | yes |

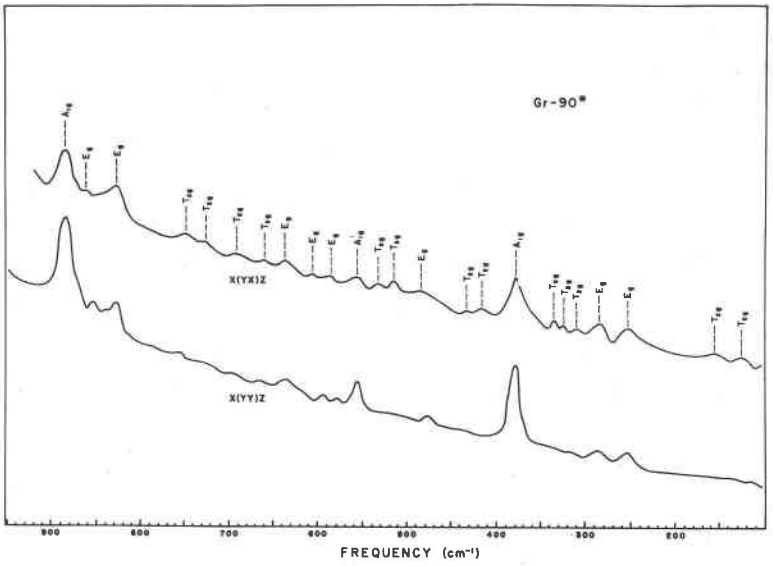


FIG. 3. Raman spectra of a grossularite (Gr-90) garnet in two polarization directions.

crossed $[x(yx)z]$. This is partly due to internal reflections, caused by internal fractures in the crystal, and to misalignment of the crystal (intentional in this case). Koningstein and Toaning-Ng (1968) have shown that, when a garnet crystal is rotated away from axis alignment with the incident and scattered radiation, the $E_g$ polarizability components transform to all possible quadratic combinations, whereas the $A_{1g}$ polarizability components remain the same. In Figure 3, the $E_g$ modes have nearly the same intensity under both experimental conditions, while the three $A_{1g}$ modes decrease in intensity markedly under crossed polarizers $[x(yx)z]$. The spectra were run numerous times with more precise alignment of the crystal, and the experimental conditions outlined in Table 7 were nearly attained. The spectra in Figure 3 are used for illustration because they exhibit the most complete set of observed bands.

A summary of the assignments is given in Table 8, along with the results for YAG as determined by Hurrel *et al.* (1968). These assignments are tentative. The frequencies of the observed bands are plotted as a function of the lattice parameter in Figure 4. The lines indicate possible correlations. The assignment of these Raman bands to particular site motions is based partly on the consensus that the high-frequency bands represent molecular motions of the tetrahedra and on the site group characteristics.

TABLE 8. RAMAN ASSIGNMENTS

| Band (Gr-90) | Representation | Site motion | Band (YAG)[a] | Representation |
|---|---|---|---|---|
| 888 | $A_{1g}$ | | 857 | $T_{2g}$ |
| 859 | $E_g$ | | 783 | $A_{1g}$ |
| 826 | $E_g$ | $\nu_1$ and $\nu_3$ | 758 | $E_g$ |
| 759 | $T_{2g}$ | | 719 | $T_{2g}$ |
| 734 | $T_{2g}$ | | 714 | $E_g$ |
| 695 | $T_{2g}$ | | 690 | $T_{2g}$ |
| 662 | $T_{2g}$ | | 561 | $A_{1g}$ |
| 638 | $E_g$ | | 544 | $T_{2g}$ |
| 592 | $E_g$ | | 537 | $E_g$ |
| 570 | $E_g$ | $\nu_2$ and $\nu_4$ | 531 | $E_g$ |
| 557 | $A_{1g}$ | | 436 | $T_{2g}$ |
| 533 | $T_{2g}$ | | 408 | $T_{2g}$ |
| 516 | $T_{2g}$ | | 403 | $E_g$ |
| 483 | $E_g$ | | 373 | $A_{1g}$ |
| 426 | $T_{2g}$ | Rotatory | 340 | $E_g$ |
| 416 | $T_{2g}$ | | 310 | $E_g$ |
| 378 | $A_{1g}$ | | 296 | $T_{2g}$ |
| 348 | $T_{2g}$ | | 243 | $T_{2g}$ |
| 330 | $T_{2g}$ | $S_4$ Trans. | 218 | $T_{2g}$ |
| 312 | $T_{2g}$ | | 162 | $E_g$ |
| 287 | $E_g$ | | 144 | $T_{2g}$ |
| 257 | $E_g$ | | — | — |
| 160 | $T_{2g}$ | $D_2$ Trans. | — | — |
| 128 | $T_{2g}$ | | — | — |

[a] Hurrel *et al.* (1968).

Two of the three $A_{1g}$ Raman active modes arise from internal tetrahedral motions, one from $\nu_1$ and one from $\nu_2$. The third $A_{1g}$ mode arises from rotatory or rocking motions of the tetrahedra. There is general agreement that the $\nu_1$ would be higher in frequency than $\nu_2$, and that the rotatory modes are generally the lowest frequency. Based on this assumption, we can assign the three $A_{1g}$ modes to the site and rotatory motions. $\nu_1$ and $\nu_3$ may be tentatively listed together for purposes of illustration. The $\nu_1$ symmetric stretch yields an $A_{1g}$ and an $E_g$ type Raman active mode, while $\nu_3$ yields an $E_g$ and three $T_{2g}$ type Raman active modes. Therefore, six modes are predicted in the Raman spectra ($A_{1g}$, $2E_g$, and $3T_{2g}$). Hurrel *et al.*'s work on YAG, where the grouping of the high-frequency bands is more obvious, shows this aggregate of the six modes of $\nu_1$ and $\nu_3$ quite clearly. In the Gr-90 sample the six highest frequency modes also contain this set of $\nu_1$ and $\nu_3$ modes.

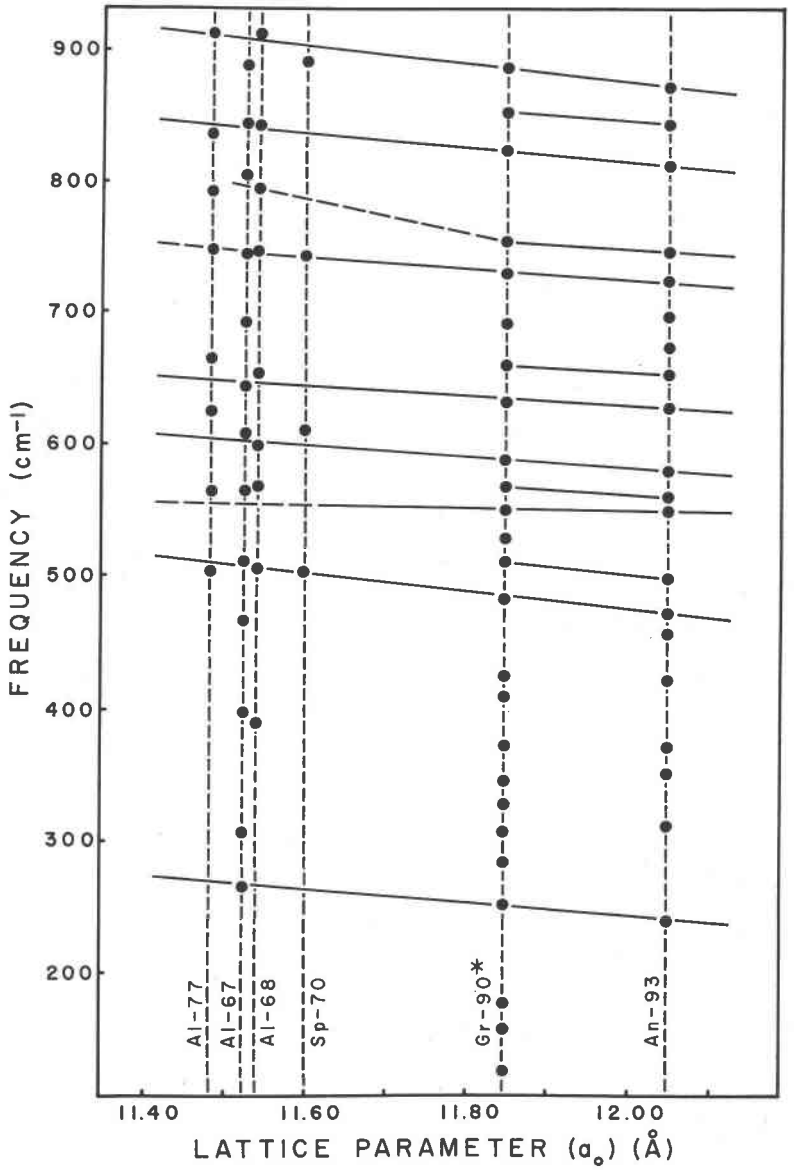


FIG. 4. Raman frequencies of garnets as a function of cell edge. Near-horizontal lines are intended to match corresponding bands.

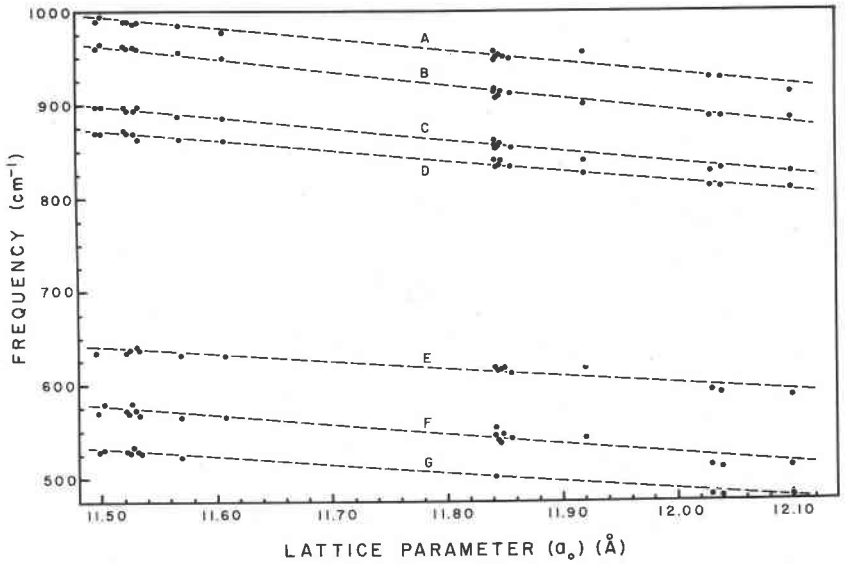


FIG. 5. Infrared frequencies of garnets as a function of cell edge.

To assign the remaining bands to specific motions as was done for $\nu_1$ and $\nu_3$ is less valid, since for these lower frequency bands the interaction between site motions could be an important factor. However, the assignment is tentatively completed by the same method as was outlined above. Such assignments are summarized in Table 8. This table includes the bands and assignments of YAG (Hurrel *et al.* 1968).

*Infrared Spectra.* Tarte (1965) and others have noted a linear relationship of the frequencies of the high-frequency infrared bands to the lattice parameter. Such plots for the first seven bands (A–G) are presented in Figure 5. It is seen that a linear relationship is indeed obtained. Bands below the frequency of *G* do not plot linearly. The tetrahedron in the natural silicate garnets remains nearly compositionally pure with the possible exception of the high-titanium garnets. It would be expected, therefore, that frequency changes of those bands representing essentially pure internal motions of the tetrahedra would be due to bond length changes, and as shown later, to differences in factor group splitting (also related to bond length changes). Bond length changes should result in linear frequency shifts of the bands as a function of the lattice parameter. Therefore, the seven bands A–G can reasonably be assigned to the tetrahedral site.

Similar plots of the frequencies of the remaining bands against the

TABLE 9. INFRARED ASSIGNMENTS

| Band | Site | Site motion |
|---|---|---|
| A | $S_4$ | |
| B | $S_4$ | $\nu_3$ |
| C | $S_4$ | |
| D | $S_4$ | |
| E | $S_4$ | |
| F | $S_4$ | $\nu_2$ and $\nu_4$ |
| G | $S_4$ | |
| H | $S_6$ | — |
| I | $S_6$ | — |
| J | $D_2$ | — |
| K | $D_2$ | — |
| L | — | — |
| M | — | — |
| N | — | — |
| O | — | — |
| P | — | — |
| Q | — | — |

average radii of the ions occupying the octahedral and dodecahedral (cubal) sites and against the average weight of the ions occupying these sites indicate that bands *H* and *I* can be related to the octahedral site, and bands *J* and *K* to the dodecahedral (cubal) site. The remaining bands do not yield reasonable plots for any parameter or are observed in too few specimens to observe valid variations, and thus cannot be assigned. These site assignments are summarized in Table 9 and are similar to those found by Tarte (1965).

Based on the assignments of Table 6, we would expect three infrared-active tetrahedral stretching vibrations at high frequencies. The group of four bands (A-D) at high frequencies consist of three very strong bands (B, C and D) and a weak shoulder (A) [Fig. 1]. The origin of the A band is not clear at the present time. The various rare earth garnets (McDevitt, 1969) exhibit only the expected 3 bands in this region.

The bands *E–G* can be related to the $\nu_2$ and $\nu_4$ infrared-active modes by analogy to the Raman spectra. Four bands are predicted from these modes; however, due to the strong interactions of the lower bands between site motions, the fourth member cannot be definitely identified.

## STRUCTURAL CORRELATIONS

Based on the assignments in the previous sections, some structural characteristics of the tetrahedral site can be determined. The infrared

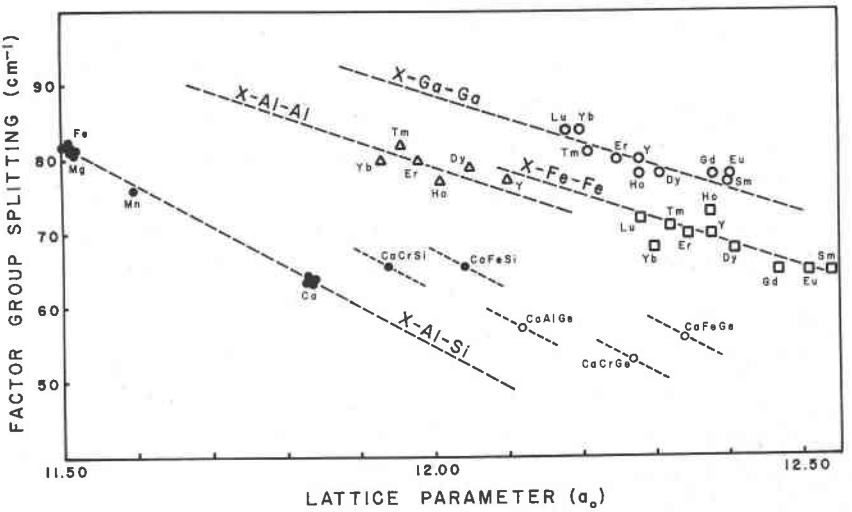


FIG. 6. The relation of the factor group splitting to cell edge for various garnets.

bands ($B$, $C$ and $D$) assigned to $\nu_3$ are of particular interest. The site and factor group splitting characteristics of this mode have been discussed. In the garnets in which the tetrahedral sites are coupled through octahedral and dodecahedral (cubal) cations, the factor group splitting would be expected to be of a larger magnitude than the site group splitting. The $S_4$ site in natural silicate garnets is only slightly distorted from true $T_d$ symmetry. Based on this, the three strong high-frequency bands in the infrared can be assigned to the two types of splitting as follows $[C-D]$ is the site group splitting, and $[B-(C+D)/2]$ is the factor group splitting. The factor group splitting values have been plotted against the lattice parameter in Figure 6. In addition, values calculated from the reported frequencies of these bands for various rare-earth garnets (McDevitt, 1969) as well as for a few germanium garnets (Tarte, 1965) are also plotted. Our data are shown as filled circles. When the 8-fold cation is varied, the factor group splittings fall onto rather nice curves for each octahedral cation. The smallest dodecahedral cations correspond to the largest factor group splitting. This implies that the coupling between tetrahedral motions is stronger when the dodecahedral distances are smaller. On the other hand, variations in the octahedral cation seem to have little effect on the factor group splitting. The series Ca-B-Si and Ca-B-Ga in Figure 6 form nearly horizontal lines, the factor group splitting being nearly constant for each set of data.

The tetrahedral site in garnets shares two of its edges with the dodeca-

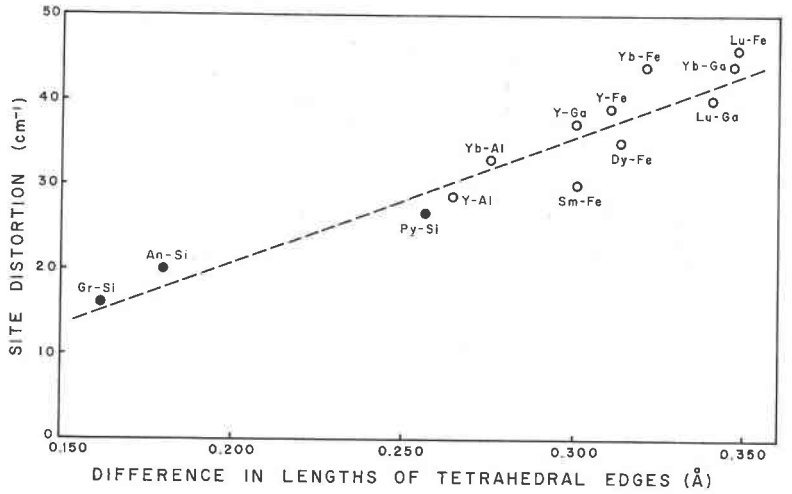


FIG. 7. Relation of the site group splitting to the distortion of the $CO_4$ tetrahedron of various garnets.

hedral (cubal) site and has four unshared edges. The length of the two shared edges is less than the value for the four unshared edges. Therefore, the difference between these two values is a measure of amount of tetrahedral distortion, since in an undistorted tetrahedron ($T_d$) all six edges would have the same length.

In Figure 7, the average value for the site group splitting of the grossularite and pyrope samples as well as the value for a number of rare-earth garnets (McDevitt, 1969) are plotted against the difference in the tetrahedral edges. The structural data are from Gibbs and Smith (1965) for pyrope, Prandl (1966) for grossularite, Novak (private communication) for andradite, and Euler and Bruce (1965) for the rare-earth garnets. The latter data are only accurate to $\pm 0.04$ Å based on their reported random experimental errors. It is seen that the infrared site splitting provides a measure of the $S_4$ distortion of the tetrahedral site.

ACKNOWLEDGMENT

This work was supported by the Air Force Materials Command, Wright-Patterson Air Force Base, under Contract No. F 33615-69-C-1105. We are indebted to G. Novak for providing us with his crystallographic data in advance of publication.

REFERENCES

DUKE, D. A., AND J. D. STEPHENS (1964) Infrared investigation of the olivine group minerals. *Amer. Mineral.* **49**, 1388–1406.

EULER, F., AND J. A. BRUCE (1965) Oxygen coordinates of compounds with the garnet structure. *Acta Crystallogr.* **19**, 971–978.

GIBBS, G. V., AND J. V. SMITH (1965) Refinement of the crystal structure of synthetic pyrope. *Amer. Mineral.* **50,** 2032–2039.

GRIFFITH, W. P. (1969) Raman studies on rock-forming minerals. Part I. orthosilicates and cyclosilicates. *J. Chem. Soc.* **1969,** 1372–1377.

HURREL, J. P., S. P. S. PORTO, I. F. CHANG, S. S. MITRA, AND R. P. BAUMAN (1968) Optical phonons of yttrium aluminum garnet. *Phys. Rev.* **173,** 851–856.

KONINGSTEIN, J. A., AND O. S. MORTENSEN (1968) Laser-excited phonon spectrum of garnets. *J. Mol. Spectrosc.* **27,** 343–350.

——— AND TOANING-NG (1968) Laser induced phonon spectrum of an oriented crystal of thulium gallium garnet. *J. Opt. Soc. Amer.* **58,** 1462–1465.

LAUNER, P. J. (1952) Regularities in the infrared absorption spectra of silicate minerals. *Amer. Mineral.* **37,** 764–784.

LYON, R. J. P. (1962a) *Minerals in the Infrared—A Critical Bibliography*, Stanford Research Institute, Menlo Park, Calif. 76 pp.

——— (1962b) *Evaluation of Infrared Spectrophotometry for Compositional Analysis of Lunar and Planetary Soils*, Stanford Research Institute, Menlo Park, Calif., Final Report on Contract NASA-NASr-49(04), 139 pp.

MARADUDIN, A. A., AND S. A. VOSKO (1968) Symmetry properties of the thermal vibrations of a crystal. *Rev. Mod. Phys.* **40,** 1–37.

MCDEVITT, N. T. (1969) Infrared lattice spectra of rare-earth aluminum, gallium and iron garnets. *J. Opt. Soc. Amer.* **59,** 1240–1244.

MITRA, S. S., AND P. J. GIELISSE (1964) Infrared spectra of crystals. *In* H. A. Symanski, ed., *Progress in Infrared Spectroscopy, Vol. 2,* Plenum Press, N.Y.

PRANDL, W. (1966) Verfeinerung der Kristallstruktur des Grossulars mit Neutronen und Rontgenstrahlbeugung. *Z. Kristallogr.* **123,** 82–116.

STUBICAN, V. S., AND R. ROY (1961) A new approach to assignment of infrared absorption bands in layer-structure silicates. *Z. Kristallogr.* **115,** 200–214.

TARTE, P. (1962) Étude infrarouge des orthosilicates et des orthogermanates. Une nouvelle methode d'interpretation des spectres. *Spectrochim. Acta*, **18,** 467–483.

——— (1965) Étude experimentale et interpretation du spectre infrarouge des silicates et des germanates. Application a des problems structuraux relatifs a l'etat solide. *Acad. Roy. Belg. Cl. Sci. Mem.* **35,** 103–119.

WHITE, W. B., AND B. A. DEANGELIS (1967) Interpretation of the vibrational spectra of spinels. *Spectrochim. Acta* **32A,** 985–995.

WICKERSHEIM, K. A. (1961) Optical and infrared spectra of the ferrites and garnets. *J. Appl. Phys.* **32,** 2055.

———, R. A. LEFEVER, AND B. M. HANKING (1960) Infrared absorption spectra of the silicate ion in the garnet structure. *J. Chem. Phys.* **22,** 271–276.

*Manuscript received, June 10, 1970; accepted for publication, July 22, 1970.*